RSC Advances

PAPER

View Article Online
View Journal | View Issue

Cite this: *RSC Adv.*, 2025, **15**, 15639

Trials of a drug release platform in near-spherical porous NiTi alloys containing a thermosensitive hydrogel as the inner coating†

Zicheng Wan,[ab] Dongyang Li,[abd] Yang Zhou,[ab] Tun Wang,[ab] Benyin Zhu,[d] Changhai Du,[d] Yimin Li[d] and Chang Shu*[abc]

Received 17th March 2025
Accepted 25th April 2025

DOI: 10.1039/d5ra01925g

rsc.li/rsc-advances

This study presents a preliminary investigation of porous nickel-titanium (NiTi) materials with controllable porosity fabricated through metal injection molding combined with the powder space-holder method (MIM-PSH). The thermosensitive hydrogel Pluronic F-127 was utilized as a drug carrier to load the anti-proliferative drug rapamycin, resulting in porous NiTi-hydrogel composite materials for controlled drug release. By tuning the NiTi matrix porosity (0%, 20%, and 40%), the system achieved precise modulation of drug loading capacity and release kinetics. Notably, the 40% porous NiTi composite exhibited a threefold increase in the drug-loading capacity and sustained release over 17 days. This hybrid design leveraged the thermoresponsive properties of the hydrogel and the tailored pore architecture to enable spatiotemporal control of rapamycin delivery, effectively inhibiting human aortic smooth muscle cell proliferation and mitigating *in vivo* vascular tissue hyperplasia. This study provides a foundational framework for the development of multifunctional biomaterial systems for vascular therapy.

1. Introduction

Currently, NiTi shape memory alloys are extensively utilized in clinical medicine owing to their remarkable properties, including superelasticity, shape memory effect, corrosion resistance, and tissue compatibility, contributing significantly to various medical applications such as orthopedic implants, orthodontic arch wire, and vascular stent.[1–3] With advancements in material processing, customized porous NiTi has emerged as a promising platform that not only mimics natural tissue architecture to enhance integration[4] but also serves as an effective volumetric reservoir for drug delivery.[5]

Conventional metal-based drug carriers, particularly non-porous NiTi alloys that rely on surface adsorption, suffer from low drug-loading efficiency and burst release. In addition, the mechanical mismatch between the drug coating and the superelastic substrate can lead to cracking, flaking, and delamination under cyclic loading.[6] To overcome these challenges, engineered porous NiTi leverages its high surface area derived from three-dimensional interconnected networks for exceptional drug-loading capacity, while tunable gradient pore architectures help regulate diffusion pathways to achieve sustained release kinetics.[7,8] Building on this foundation, the integration of hydrogels into porous architectures has attracted significant interest.[9,10] Hierarchical pores limit hydrogel swelling and promote capillary-driven infiltration, thereby extending drug release duration; meanwhile, the hydrogel enables stimuli-responsive and pulsatile delivery and covalent anchoring to pore walls, improving interfacial stability.[11] This combination enhances drug distribution and coating adhesion, effectively mitigating mechanical failure under physiological loading conditions.[12–15]

Despite recent progress, optimizing drug loading, extended release, and ensuring long-term stability remain key challenges for next-generation implantable drug delivery systems, especially in vascular applications, where porous NiTi alloys are increasingly favored. In our previous study, we developed a porous NiTi alloy featuring uniformly distributed near-spherical pores *via* metal injection molding (MIM).[16] By filling this intricate porous matrix with thermosensitive Pluronic F127 hydrogel through vacuum impregnation, we created a highly efficient drug reservoir that maximizes the use of the internal architecture for superior drug loading, significantly surpassing conventional materials while achieving sustained and controllable drug release. Our current research further explores the sustained-release performance of this novel composite system, emphasizing the synergistic integration of porous NiTi and

[a]*Department of Vascular Surgery, The Second Xiangya Hospital of Central South University, Changsha, China*

[b]*Angiopathy Institute of Central South University, Changsha, Hunan 410011, China*

[c]*Department of Cardiovascular Surgery, Chinese Academy of Medical Sciences and Peking Union Medical College Fuwai Hospital, Xicheng District, Beijing 100037, China. E-mail: shuchang@csu.edu.cn*

[d]*State Key Laboratory of Powder Metallurgy, Central South University, Changsha, 410083, China*

† Electronic supplementary information (ESI) available. See DOI: https://doi.org/10.1039/d5ra01925g

thermosensitive hydrogel to optimize drug loading and release kinetics for advanced endovascular therapy.

2. Materials and methods

2.1 Fabrication of porous NiTi

Spherical pre-alloyed NiTi powder (Ni : Ti atomic ratio of 50.49 : 49.51, D50 = 10.9 μm; Jiangsu Vilory Advanced Materials Technology, Xuzhou, China) was used as the raw material, while spherical PMMA ((C5O2H8)n; Mitsubishi Rayon Polymer Nantong, Nantong, China) served as the space holder. The PMMA powder (−200 mesh) was blended with NiTi powder for 24 hours. A multi-component polymer binder—composed of 60% paraffin, 35% high-density polyethylene, and 5% stearic acid—was used for the injection molding process. The NiTi powder, space holder, and binder were mixed at 170 °C for 2 hours under Ar gas flow to prepare the feedstock. Injection molding was then performed, followed by solvent debinding in dichloromethane at 40 °C for 12 hours to remove the solvent-based binder. Subsequent thermal debinding was performed at a maximum temperature of 600 °C under an Ar atmosphere. Finally, the samples were sintered in a vacuum furnace at 1240 °C for 6 hours under a pressure of 10^{-4} Pa. The process involved several steps, including raw material blending, injection molding, debinding, and sintering (Fig. 1). Further details on near-spherical porous NiTi alloys are available in our previous study.[16,17]

2.2 Sample preparation

As shown in Table 1, porous NiTi samples with porosities PMMA addition of 20% (Group N2) and 40% (Group N3) and similar pore sizes were fabricated using a powder metallurgy process as previously described.[16] Dense NiTi samples (0% porosity addition) were produced using the same powder metallurgy process and used as controls (Group N1). For the drug release test, cylindrical samples measuring Φ 4 mm × 5 mm were extracted from these three NiTi alloys, while cylindrical samples with dimensions of Φ 4 mm × 0.4 mm (thickness) were used for cell culture. For rat aorta implantation, cylindrical samples with diameters of 0.2 mm and lengths of 3 mm were used. The surface of the sample was polished with 1200 to 2000-grit waterproof emery paper and then a SiO_2 suspension, followed by cleaning in acetone, alcohol, and deionized (DI) water with ultrasound for 10 minutes each, and subsequent drying in an ambient atmosphere.

Table 1 Pore parameters of the porous NiTi alloys

Sample	PMMA addition (vol%)	Average pore size (μm)	Porosity (%)
N1	0	—	3.3
N2	20	40.8	20.8
N3	40	44.9	34.9

2.3 Drug loading

Pluronic F127 (PEO_{99}–PPO_{65}–PEO_{99}, triblock copolymer, MW 12,500 Da; Poloxamer 407) was procured from Sigma-Aldrich, and rapamycin ($C_{51}H_{79}NO_{13}$) was obtained from Aladdin. A model drug solution containing 50% w/v rapamycin was prepared in acetone. The thermosensitive hydrogel matrix was fabricated by dissolving Pluronic F127 powder in physiological saline (0.9% NaCl) under continuous agitation at 0 °C to achieve

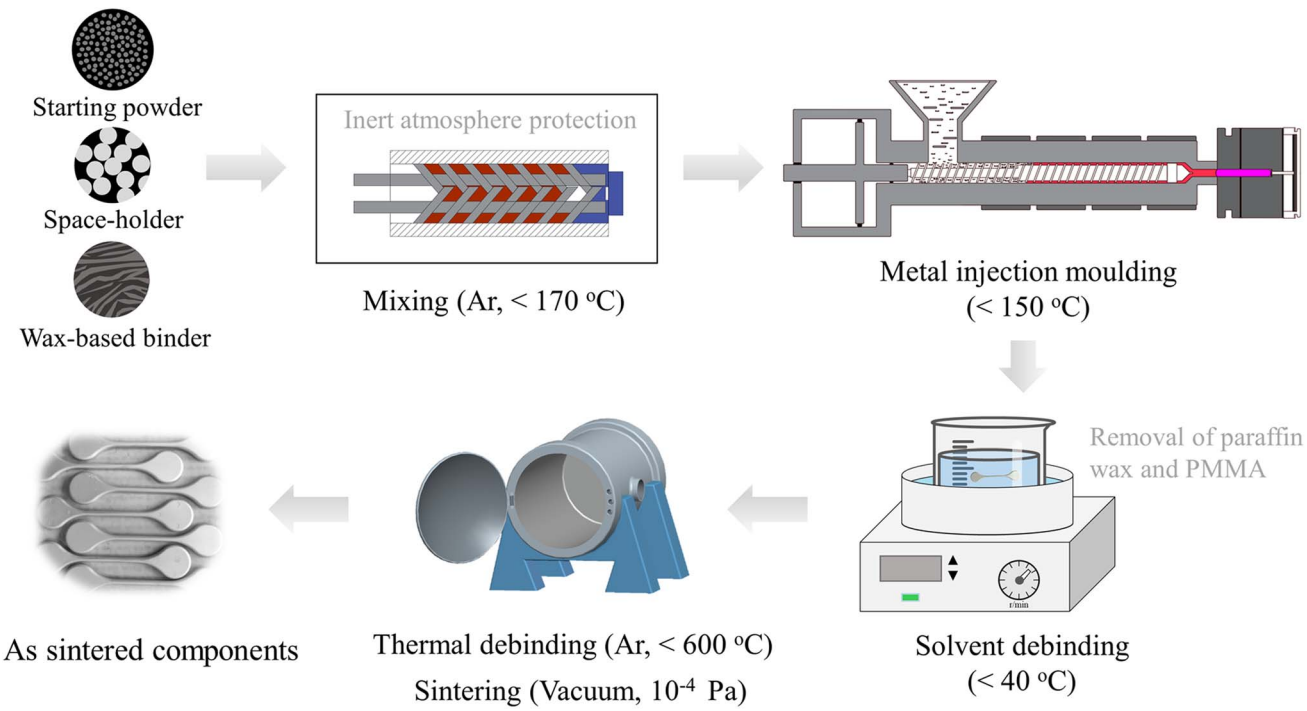

Fig. 1 Schematic of the MIM process for producing porous NiTi alloys. (Reproduced with permission from ref. 16 Copyright 2025, Elsevier).

a 20% w/v concentration. This low-temperature protocol ensured the complete dissolution of the triblock copolymer while preserving its thermoresponsive properties. The rapamycin-acetone solution was then homogeneously blended with the 20% F127 solution at 0 °C, followed by controlled solvent evaporation to remove acetone residues, as illustrated in Fig. 2A. For drug-loaded material preparation, porous substrates were impregnated with a hydrogel/rapamycin mixture in a vacuum chamber (DZ-1BCIV, Tianjin TEST, China). The vacuum pressure was maintained at 10^{-1} Pa for 4 hours to ensure thorough penetration into the porous architecture. Subsequently, temperature-induced gelation was triggered by incubating the impregnated scaffolds at 37 °C for 15 minutes, leveraging the reverse thermal gelation characteristics of Pluronic F127. Finally, the scaffolds underwent thermal drying, followed by the mechanical removal of excess surface hydrogel using soft tissue wipes post-gelation (Fig. 2B).

2.4 Structural characterization

The structural characterization of porous NiTi implants before and after drug loading involved cross-sectional scanning electron microscopy (SEM) analysis to examine their structural characteristics. The SEM images provided detailed insights into the post-treatment morphology and porosity of the materials. Additionally, energy-dispersive X-ray spectroscopy (EDS) analysis was employed to further investigate the elemental composition of the material cross-sections. This analytical technique enabled the precise identification and quantification of the elements present within the samples, providing valuable information regarding the distribution and incorporation of the elements after gel processing.

2.5 Assessment of rapamycin release Pluronic F127-rapamycin loaded porous NiTi

Drug release from the drug-loaded porous NiTi implants was assessed by immersing the samples in 5 mL of phosphate-buffered saline (PBS), with the released drug quantified using high-performance liquid chromatography (HPLC). To capture the release dynamics, measurements were taken at frequent intervals within the first 24 hours to monitor the initial burst release and subsequently every 2 days to evaluate the sustained release phase, continuing until no further drug was detected in the PBS. The absorbance was recorded at a peak wavelength of 278 nm, and the drug concentration was determined based on a pre-established calibration curve. In the drug release study, the release efficiency was calculated as the cumulative release percentage, which is the ratio of the total released drug amount to the maximum drug loading capacity.

2.6 Inhibitory effects of Pluronic F127-rapamycin loaded porous NiTi on cell proliferation

Human aortic smooth muscle cells (HASMCs; Otwo Biotech Inc., Shenzhen, Guangdong, China) were cultured in Smooth Muscle Cell Medium (SMCM; ScienCell, CA, USA) supplemented with 5% fetal bovine serum (FBS) and 1% (v/v) penicillin–streptomycin. Cells were maintained in a humidified incubator at 37 °C with 5% CO_2. HASMCs were then seeded onto Pluronic F127-rapamycin loaded cylindrical samples with dimensions of Φ 4 mm × 0.4 mm (thickness) at a density of 2×10^4 cells per well and cultivated for 2 days. The samples were stained with FITC-Phalloidin (Yeasen, Shanghai, China) for 30 minutes, followed by counterstaining with 4′,6-diamidino-2-phenylindole (DAPI; Biosharp, Hefei, China) for 3 minutes at room temperature. The cytoskeletal organization of HASMCs was visualized using a fluorescence microscope (Olympus BX53, Tokyo, Japan). For each sample, five randomly selected fields were examined, and cellular and nuclear areas were quantified using ImageJ software.

To evaluate the cytotoxicity of NiTi carriers (without hydrogel/drug components), an extraction-based assay was performed. After polishing and cleaning, dense and porous NiTi samples were incubated in a complete culture medium at 37 °C for 72 hours (extraction ratio of 1.25 cm^2 mL^{-1}). Human aortic smooth muscle cells (HASMCs) were seeded at 2×10^3 cells per well in 96-well plates and allowed to adhere for 24 hours. The medium was then replaced with NiTi extraction medium and incubated for another 24 hours. Cell viability was assessed using the CCK-8 assay, with absorbance measured at 450 nm.

2.7 Inhibitory effects of Pluronic F127-rapamycin loaded porous NiTi on neointimal hyperplasia

This study aimed to simulate stent-induced vascular injury by externally fixing a porous NiTi alloy to the aortic wall in rats. Similar to stent implantation, disrupting endothelial integrity and triggering smooth muscle cell activation and intimal

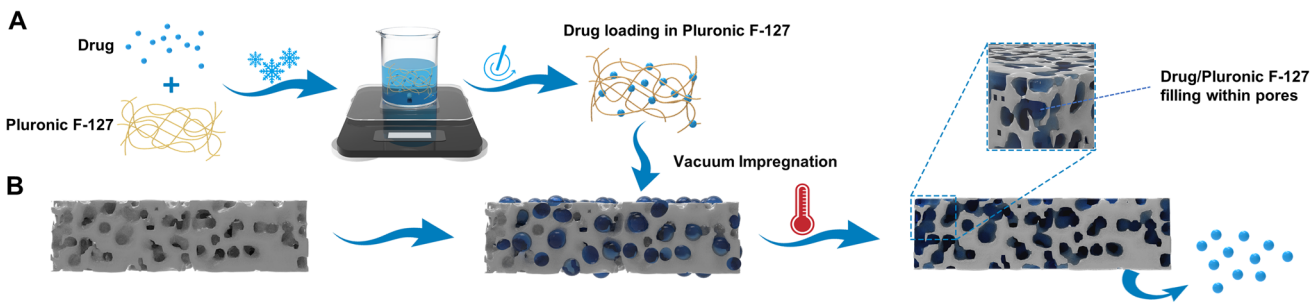

Fig. 2 Scheme of porous NiTi implants modified with Pluronic-F127. (A) Mixing and thoroughly blending the drug (rapamycin) with the Pluronic hydrogel at 4 °C. (B) Using vacuum impregnation method to thoroughly fill the hydrogel into the porous structure, followed by sustained drug release at physiological temperature.

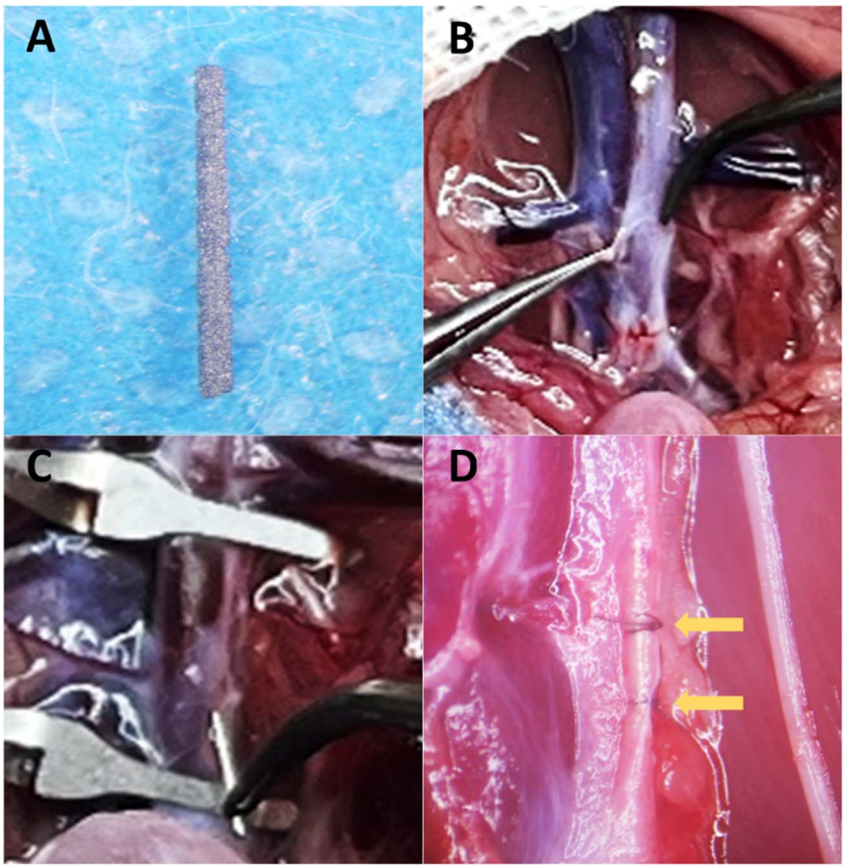

Fig. 3 Establishment of a metal-induced aortic intimal hyperplasia model. (A) Porous NiTi alloy segment used for implantation. (B) Surgical exposure of the aorta (C) A 0.2 mm incision was made on the side wall of the aorta. A cylindrical NiTi sample (0.2 mm in diameter and 3 mm in length) was then inserted through the incision. (D) Sample was securely fastened to the inner wall of the infrarenal aorta using 10–0 nylon sutures. Postoperative evaluation of the implanted alloy segment (indicated by yellow arrows).

hyperplasia,[18,19] this model induced endothelial damage. Twelve male Sprague-Dawley rats (300–350 g) received Pluronic F127 hydrogel-coated rapamycin/NiTi implants in the infrarenal aorta. Animals were housed under standard conditions (25 °C, 12 h light/dark) with ad libitum access to food and water, following NIH guidelines. Under isoflurane anesthesia, a midline abdominal incision exposed the infrarenal aorta. The aorta was isolated 2 mm distal to the renal artery with ligated lumbar branches. Fig. 3 shows the establishment of a metal implantation-induced aortic intimal hyperplasia model. (A) A porous NiTi alloy segment is used for implantation. (B) Surgical exposure of the aorta (C). A 0.2 mm incision was made in the lateral wall of the aorta, through which a cylindrical NiTi sample (0.2 mm in diameter and 3 mm in length) was inserted. (D) The sample was then securely anchored to the inner wall of the infrarenal aorta using 10–0 nylon sutures. Postoperative evaluation of the implanted alloy segment (indicated by yellow arrows). Rats received daily heparin (100 IU kg^{-1}, 7 days) without immunosuppressants/antibiotics.

2.8 Histological evaluation of neointimal formation at the NiTi implantation site in the aortic wall

Rats were euthanized, and the aortic segments containing the NiTi implants were harvested for analysis two weeks postoperatively. The tissues were fixed in 4% paraformaldehyde (PFA), dehydrated through a graded ethanol series, and embedded in paraffin. Paraffin-embedded samples were sectioned at a thickness of 4 μm and stained with Masson's trichrome (Solarbio, China) to assess neointimal formation following implantation. The entire neointimal area and the thinnest neointimal thickness were automatically measured using ImageJ software. In porous NiTi constructs, the neointima tends to infiltrate the pores, leading to a nonuniform thickness. Therefore, by quantifying both the overall area and the minimal thickness, we ensured an accurate assessment of the neointima.

2.9 Statistical analysis

All quantitative data are presented as mean ± standard deviation (SD). Statistical analyses were conducted using GraphPad Prism version 8.0.2. One-way ANOVA and *t*-tests were used to assess statistical significance, with *p*-values less than 0.05 considered statistically significant.

2.10 Study approval

All animal experimental procedures were reviewed and approved by the Institutional Animal Care and Use Committee

of Second Xiangya Hospital, Central South University (Approval No. 20220123). All experiments were conducted in strict accordance with approved guidelines.

3. Results

3.1 Characterization of porous NiTi using thermosensitive hydrogel/rapamycin

As shown in Fig. 4, the varying shapes of the temperature-sensitive hydrogels in different states are observable. The morphology of the prepared porous NiTi substrates was characterized by SEM, and a typical cross-sectional image of the thermosensitive hydrogel loading in the porous NiTi structure is presented in Fig. 5. Internal electron microscopy images of porous NiTi columnar materials with 20% and 40% porosity after vacuum impregnation are presented. Through EDS elemental mapping (Fig. 6), black–gray regions are predominantly characterized by the distribution of carbon and oxygen, while other areas are dominated by nickel and titanium.

3.2 Drug release of porous NiTi with thermosensitive hydrogel/rapamycin *in vitro*

The comparative drug release profiles of Pluronic F127-Rapamycin loaded porous NiTi implants with different porosity as a carrier are shown in Fig. 7. The initial burst release within the first 24 hours and the overall drug release profile are presented. The release characteristics are summarized in Table 2, which includes the release efficiency (% drug released) at specific time points (1, 7, 14, and 31 days) and the time required for complete drug release. In the control group, the release kinetics exhibited a biphasic pattern, with a substantial proportion (44%) of the drug released within the first 24 hours, followed by a slower, sustained release over the subsequent 7 days. For the groups with porosities of 20% and 40%, the overall sustained release durations were 13 days and 17 days, respectively. However, with the increase in porosity, not all drugs were released, with cumulative drug release rates reaching 72.2% and 68.2%, respectively. Regarding drug loading capacity, significant differences were observed in the maximum loading capacity of the three different groups. The maximum loading capacity of porous NiTi with a porosity of 40% was approximately 4.44 times that of dense NiTi, while that of porous NiTi with a porosity of 20% was approximately 2.82 times that of dense NiTi.

3.3 Inhibitory effects of Pluronic F127-rapamycin loaded porous NiTi on HASMC proliferation

The proliferation of HASMCs on Pluronic F127–rapamycin-loaded porous NiTi samples was evaluated using nuclear staining (Fig. 8A). Quantitative analysis (Fig. 8B) showed that the number of cells in group N1 was higher than in groups N2 and N3, with group N2 also showing a higher cell count than group N3. The cell morphology on all sample surfaces was observed *via* F-actin staining (Fig. 8C). HASMCs cultured on N1 and N2 cells exhibited regular cellular morphology with clearly visible nuclei and peripheral filament bands. In contrast, cells on N3 exhibited a contracted morphology in both the cytoplasm and nucleus, along with pronounced disruption of the

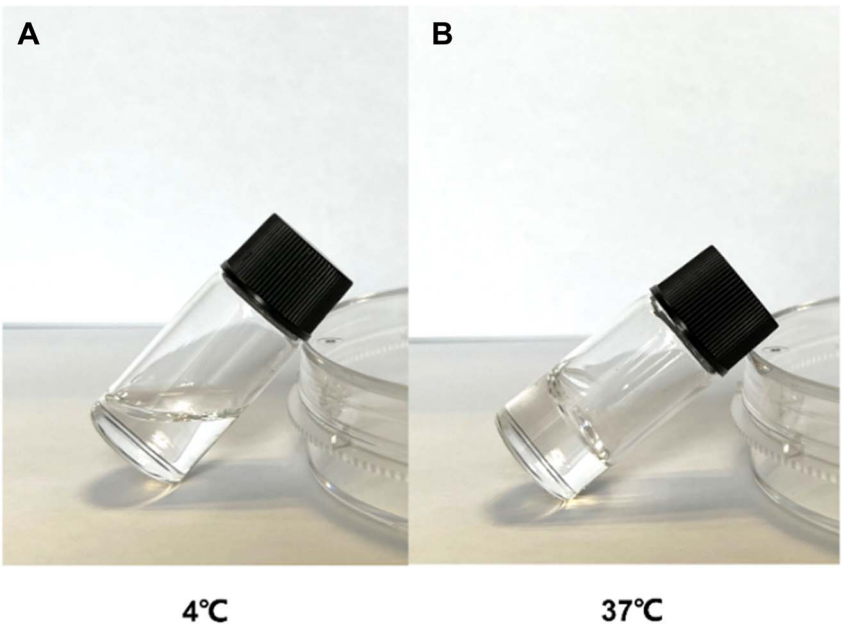

Fig. 4 Variations in the morphology of the hydrogel at different temperatures. (A) Photograph of a 20 wt% Pluronic F127 (poloxamer 407) solution at 4 °C, where it remains in a relatively low-viscosity sol state. At this temperature, the hydrophobic poly(propylene oxide) (PPO) segments are sufficiently solvated by the hydrophilic poly(ethylene oxide) (PEO) blocks, preventing extensive micellization and network formation. (B) Photograph of the same Pluronic F127 solution at 37 °C, where increased hydrophobic interactions among the PPO segments lead to micelle aggregation and physical crosslinking, resulting in a gel-like network. This temperature-triggered sol–gel transition is a hallmark of PEO–PPO–PEO triblock copolymers and underpins their widespread use in materials science and biomedical applications, including injectable hydrogels, drug delivery vehicles, and tissue engineering scaffolds.

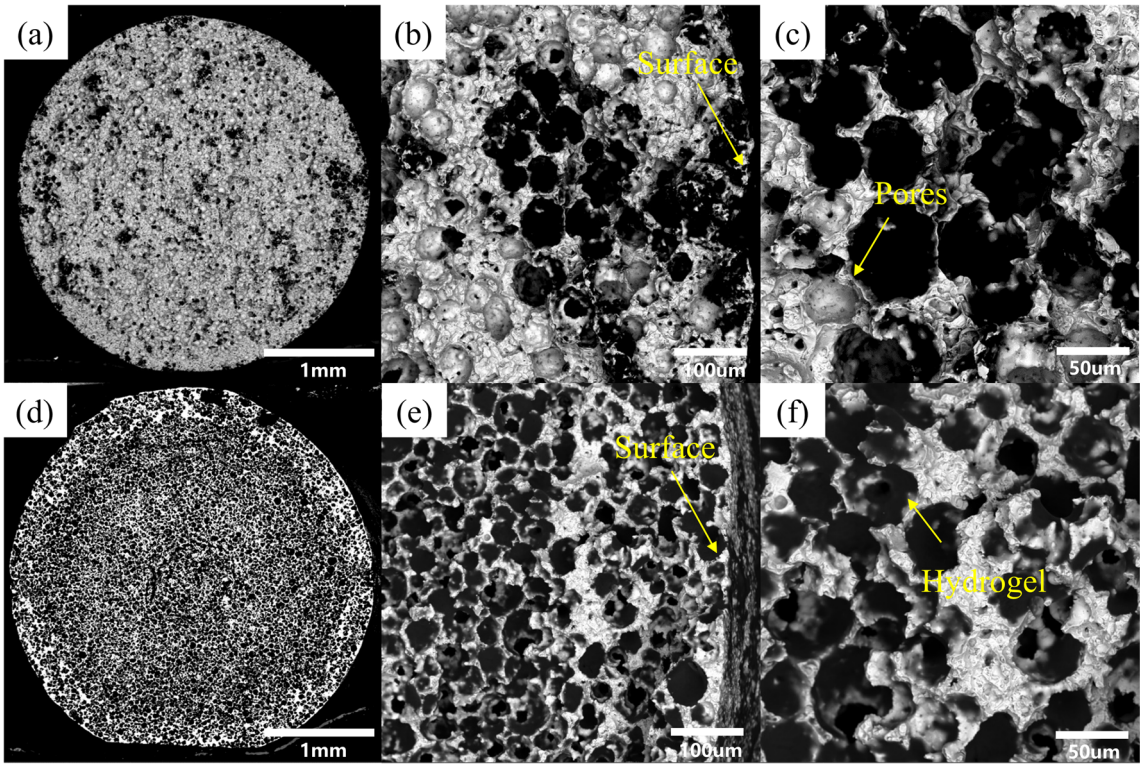

Fig. 5 Scanning electron microscopy (SEM) characterization of porous NiTi implants with hydrogel loading. (a–c) 40% porosity sample low-to high-magnification images reveal a homogeneous distribution of near-spherical pores within the NiTi matrix. Partial hydrogel coverage (black regions) was observed, with hydrogel localized to pore peripheries, leaving central pore regions exposed. (d–f) 40% porosity sample with increased pore interconnectivity facilitates extensive hydrogel infiltration, as evidenced by near-complete pore filling (black hydrogel domains). The hydrogel adheres uniformly to the pore walls, forming a conformal coating.

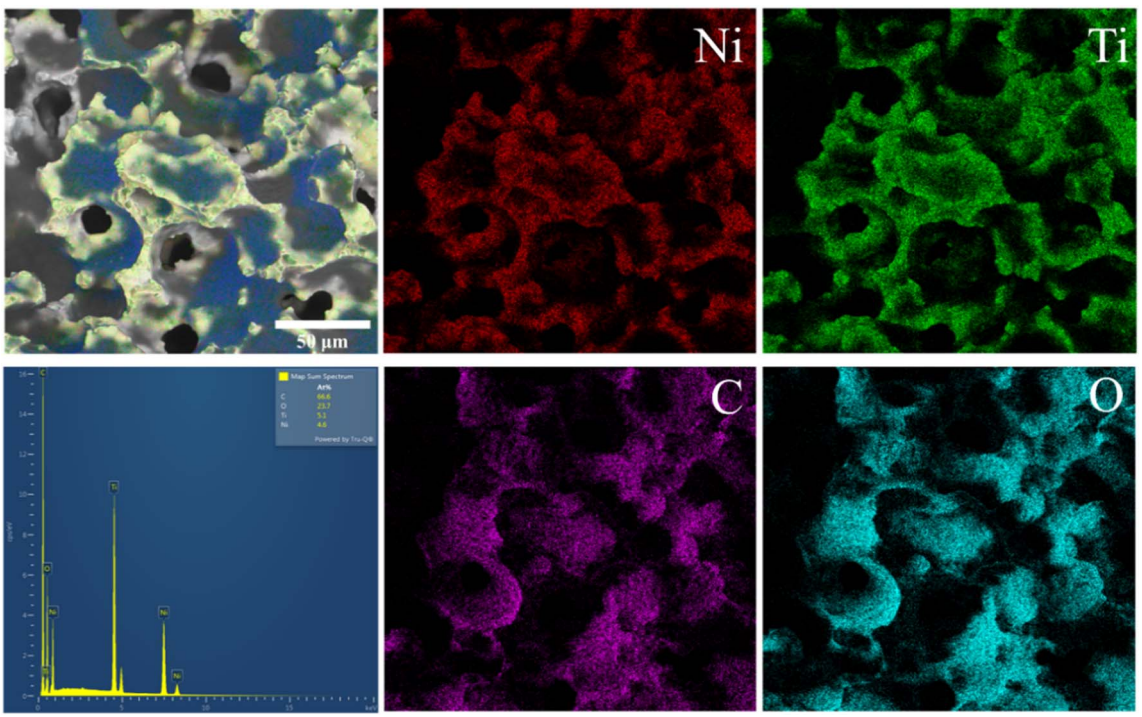

Fig. 6 EDS spectrum and elemental mapping reveal distinct carbon (C) and oxygen (O) enrichment within the pore interiors, in contrast to the bulk NiTi matrix. This localized C/O distribution corresponds to the black hydrogel residues observed in the SEM images, confirming successful hydrogel retention within the pores during loading. The Ni/Ti ratio remained homogeneous throughout the porous architecture, demonstrating the preservation of structural integrity without elemental segregation.

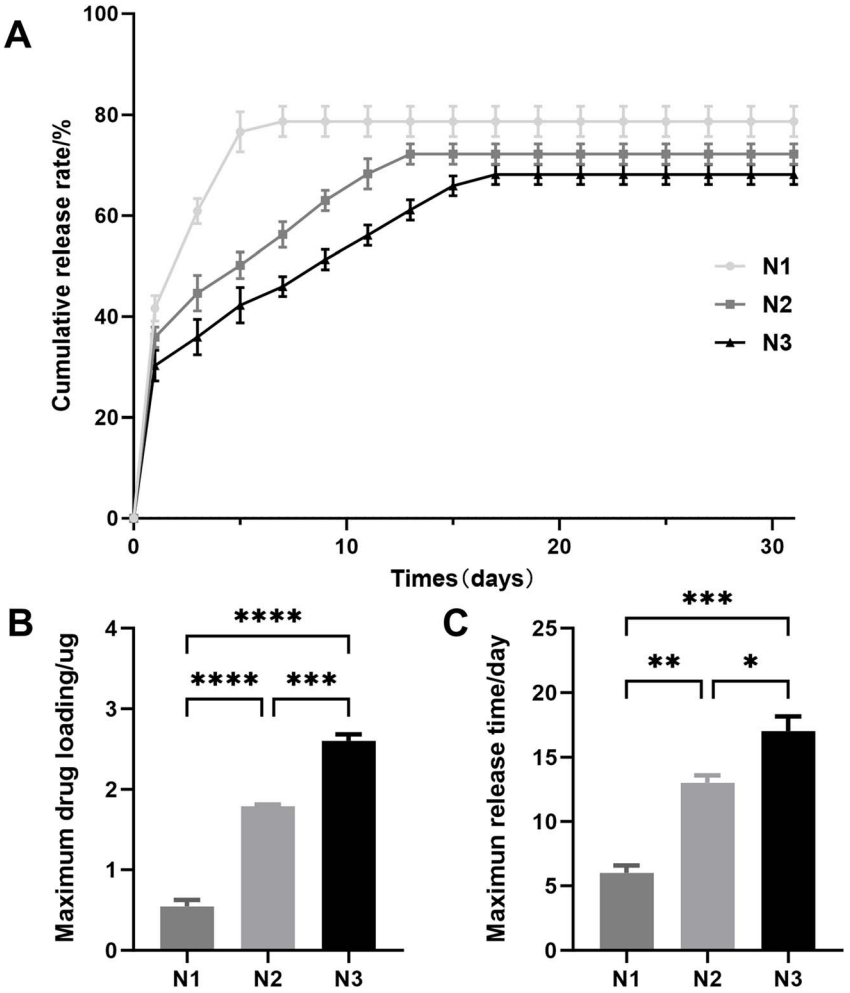

Fig. 7 *In vitro* release of F127/rapamycin-loaded porous NiTi. (A) Cumulative release rate of F127/rapamycin-loaded porous NiTi with different porosities. (B) Maximum release time of NP-rapamycin NiTi with different porosities. (C) Maximum rapamycin loading of porous NiTi with different porosities. *, **, ***, and **** indicate $p < 0.05$, $p < 0.01$, $p < 0.001$, and $p < 0.0001$, respectively.

microfilament structure. Quantitative analysis (Fig. 8D) further confirmed that the cellular area in groups N1 and N2 was significantly larger than that in group N3. Before evaluating the anti-proliferation effects, cytocompatibility testing *via* the CCK-8 extract assay demonstrated that bare porous NiTi exhibited no significant differences in cytotoxicity (ESI Fig. 1†).

3.4 Inhibitory effects of F127/rapamycin-loaded NiTi on neointimal hyperplasia

Masson staining of aortic tissues 2 weeks post-implantation revealed distinct neointimal remodeling across F127/rapamycin-loaded NiTi implants with varying porosity (Fig. 9). In all groups, the neointima-media boundary was demarcated by a yellow dashed line, clearly separating the collagen-rich neointima (blue) from the underlying medial layer (red smooth muscle cells). Significant differences in neointimal area and thickness were observed between the different porosity groups. The neointimal thickness and area were significantly lower in the N3 group than in the N1 and N2 groups, whereas the neointimal thickness in the N2 group was also significantly lower than that in the N1 group. These findings indicate that increasing porosity enhances the loading capacity of rapamycin, thereby exerting a stronger inhibitory effect on neointimal hyperplasia.

4. Discussion

In this study, we developed a porous NiTi metal drug delivery platform with a thermosensitive hydrogel as the inner coating. We aimed to address the common challenges associated with traditional drug coating or eluting techniques, such as cracking, delamination, and peeling, that occur due to the material's elastic strain during the drug-loading process. To address these issues, we used a vacuum impregnation method to introduce the Pluronic-127 thermosensitive hydrogel into the porous structure of the materials, enabling slow and sustained drug release. This method facilitated successful drug delivery to the core of the material at low temperatures, with the hydrogel solidifying under normal physiological conditions. As shown in Fig. 10, the release of entrapped drugs (*e.g.*, rapamycin) was

Table 2 Drug release characteristics of NiTi implants with different porosities loaded with rapamycin/PF127. (Mean ± SD, $n = 3$)

Porosity	Drug release (%)				100% drug released (no. of days)
	1 day	7 days	14 days	31 days	
N1	42.0 ± 2.5	79.0 ± 3.0	79.0 ± 3.0	78.7 ± 3.0	7
N2	35.9 ± 2.0	56.3 ± 2.5	72.2 ± 2.0	72.2 ± 2.0	13
N3	30.3 ± 3.0	46.0 ± 2.0	65.9 ± 2.0	68.2 ± 2.0	17

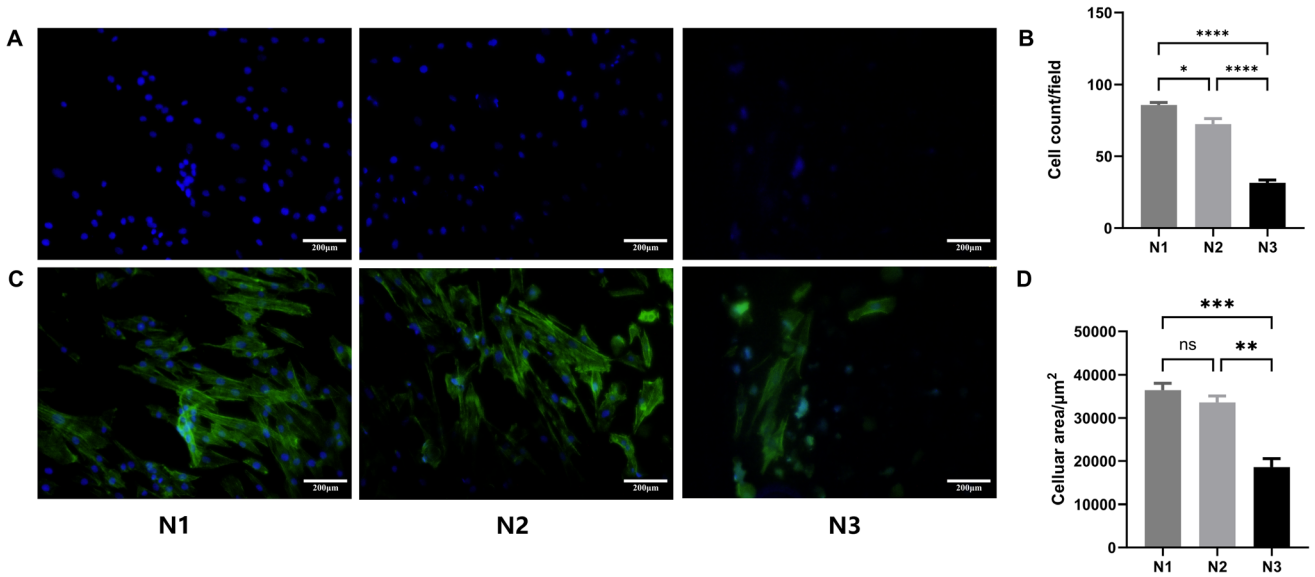

Fig. 8 Inhibitory effects of F127/rapamycin-loaded porous NiTi on HASMC proliferation. (A) Fluorescence images of HASMCs cultured on NiTi samples with varying porosities for 2 days. (B) Bar graph showing the HASMC cell count on NiTi surfaces with different porosities. (C) Fluorescence images showing the cytoskeleton organization of HASMCs cultured on NiTi samples with varying porosities for 7 days. (D) Bar graph showing the cellular areas of HASMCs on NiTi surfaces with different porosities. *, **, ***, and **** indicate $p < 0.05$, $p < 0.01$, $p < 0.001$, and $p < 0.0001$, respectively.

regulated by reducing the swelling of the inner-pore gel. As the outer hydrogel gradually degrades, stored drugs are released from the inner pores, acting as a reservoir and enabling slow, sustained drug release.

Based on our previous study on MIM-manufactured NiTi alloys with uniform near-spherical pores.[16] The current MIM-PSH strategy achieves decoupled control of pore architecture: pore dimensions replicate the original PMMA template size (68.5 μm initial particles), with post-sintering shrinkage reducing final pore diameters to 40.8 μm (P20, 20 vol% PMMA) and 44.9 μm (P40, 40 vol% PMMA). The porosity was independently modulated *via* the volumetric addition of PMMA, leading to a significant increase from 20.8% to 34.9% with minimal pore size variation (±4 μm). This stability is enabled by the multi-step sintering densification process, which preserves the pore morphology while decoupling the pore size control (template-driven) from the porosity modulation. The resulting structural precision ensures uniform pore geometry—pore size governs diffusion-mediated processes. As shown in Fig. 5, a high-resolution cross-sectional SEM image of the porous NiTi layer reveals uniformly sized spherical micropores and presents the cross-sections of Group N2 and Group N3 before and after treatment with hydrogel solution. Group N2 (20% porosity) showed incomplete hydrogel penetration along the thickness direction, likely due to closed pores or limited interconnectivity hindering uniform diffusion, leaving the material core partially unfilled. In contrast, Group N3 (40% porosity) achieved full-thickness infiltration *via* interconnected SHPs, as evidenced by a uniform black–gray colloidal substance spanning the entire cross-sectional thickness under vacuum impregnation. EDS mapping confirmed homogeneous F127 distribution in N3, highlighting that pore connectivity—not just porosity—determines hydrogel penetration depth and thickness-resolved drug loading efficacy. In our previous studies,[16] NiTi alloys with different porosities were prepared using metal injection molding combined with the powder space-holder method (MIM-PSH). Although P20 and P40 exhibited similar pore sizes, P40 exhibited a significantly higher pore distribution density. The interconnected porous structure primarily results from the removal of PMMA, leaving behind space-holder pores (SHPs).[16] Thus, for this study, porous NiTi with a pore diameter of 40 μm was prepared to maximize its drug-loading capacity.

Polymeric systems are considered effective drug carriers due to two primary advantages: they provide a framework for

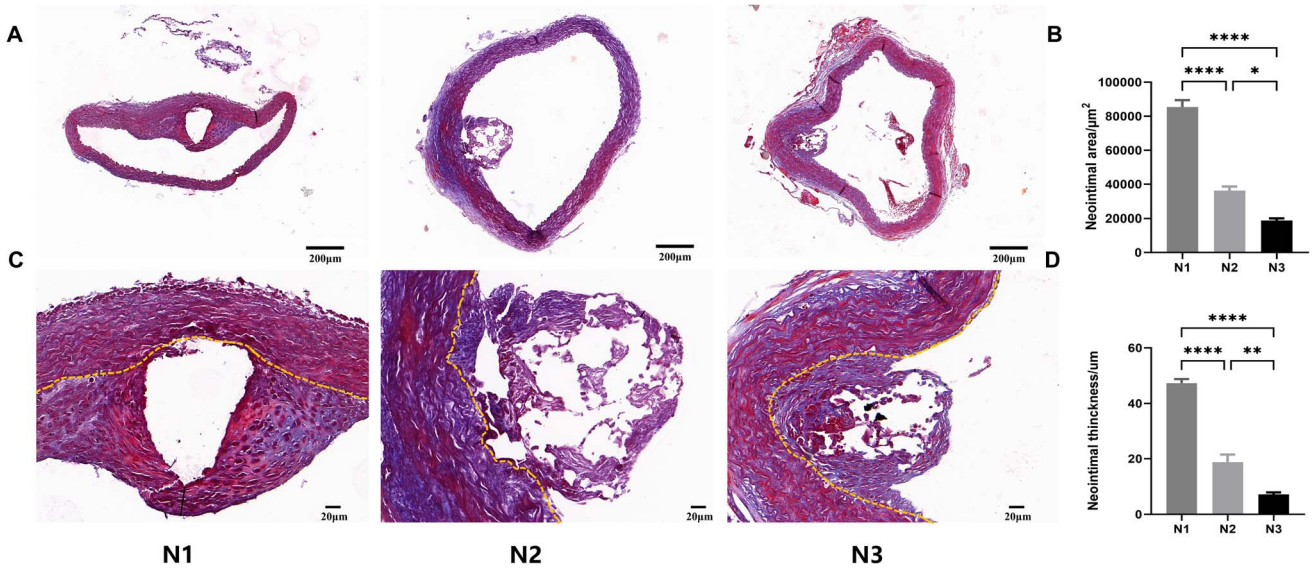

Fig. 9 Inhibitory effects of F127/rapamycin-loaded porous NiTi on neointimal hyperplasia. (A) Low-magnification overview of vascular remodeling at the implantation site, where neointimal hyperplasia (arrows) is prominently developed. The neointimal region is characterized by dense collagen deposition (blue) and disorganized cellular proliferation. (B) Bar graph showing the neointimal area in F127/rapamycin-loaded porous NiTi implants with different porosities (C) Higher magnification image highlighting the microarchitecture of the hyperplastic tissue: collagen bundles (blue) form a fibrous network intermingled with spindle-shaped smooth muscle cells (red cytoplasmic staining) and scattered inflammatory cells. Yellow dashed lines denote the neointima-media interface. Compared with the F127/rapamycin-loaded dense NiTi group, the porous NiTi groups exhibit a significant reduction in neointimal thickness and improved collagen fiber alignment, suggesting that the porous architecture may enhance drug efficacy by promoting uniform drug distribution and tissue integration. (D) Bar graph showing the neointimal thickness in F127/rapamycin-loaded NiTi implants with different porosities. *, **, ***, and **** indicate $p < 0.05$, $p < 0.01$, $p < 0.001$, and $p < 0.0001$, respectively.

controlled drug release and protect the drug from degradation before it exerts its therapeutic effect.[20] In previous studies, the physical mechanisms of drug release have been described as involving several processes: diffusion through a polymer layer, dissolution or degradation of the polymer, permeation pressure, and ion exchange. Among these, hydrogel coating involves the modification of balloon surfaces with hydrogels as a carrier layer for various medicines. These hydrogel layers are highly hydrophilic and contain a large amount of water, which enhances their bioadhesive properties. Lee S. *et al.* proposed the use of hydrogel-coated balloon catheters as drug reservoirs for the treatment of coronary artery disease (CAD).[21] In our study, we adopted the thermo-sensitive hydrogel Pluronic F-127, a well-recognized temperature-sensitive polymer approved by the United States Food and Drug Administration as being non-toxic. Aqueous solutions of Pluronic F-127 exhibit thermoreversible properties, undergoing a phase transition from a low-viscosity transparent solution at 4–5 °C to a solid gel at body temperature. By exploiting this property, at low temperatures, the F127 hydrogel remains in a sol state, allowing molecular chains to diffuse freely and rendering the solution fluidic. Through physical mixing with simulated drugs, as the temperature increases beyond the critical temperature range (typically around 20–40 degrees Celsius), a phase transition leads to molecular chain entanglement, forming a network structure that entraps drugs within the hydrogel.[22–24] Currently, this thermo-sensitive hydrogel has been extensively reported to serve as an excipient with continuous drug release in numerous clinical trials[25,26].

With the widespread application of shape memory alloys for drug delivery, releasing pharmaceutical agents from the surface of these carriers has shown promising progress in the field of endovascular materials.[27] However, there are limitations in delivering a sufficient amount of drugs within an appropriate time frame. Typically, only a small portion of the drug is released, and this often proves insufficient.[28] Additionally, issues such as cracking, flaking, and delamination frequently occur with shape memory alloys.[6] From a structural perspective, traditional drug-eluting or drug-coating stents commonly use drug carriers constructed using surface coatings or surface micropores.[29–31] These platforms may include surface titanium dioxide nanotubes for drug loading or polymer coatings, among others.[6,24] Drug release from F127-based drug delivery systems primarily relies on the disassembly of micellar structures and temperature sensitivity, while being influenced by drug dissolution and diffusion. In this study, we aimed to alleviate these issues using inner pores drug loading. SEM images demonstrated that our drug-loading method effectively incorporated the drug into both the surface and pores of the NiTi material. In terms of drug-loading capacity, there were significant differences among materials with three different types of porosity. The maximum drug-loading capacity of porous NiTi with 40% porosity was approximately 4.44 times that of dense NiTi, whereas the maximum drug-loading capacity of porous NiTi with 20% porosity was approximately 2.82 times that of dense

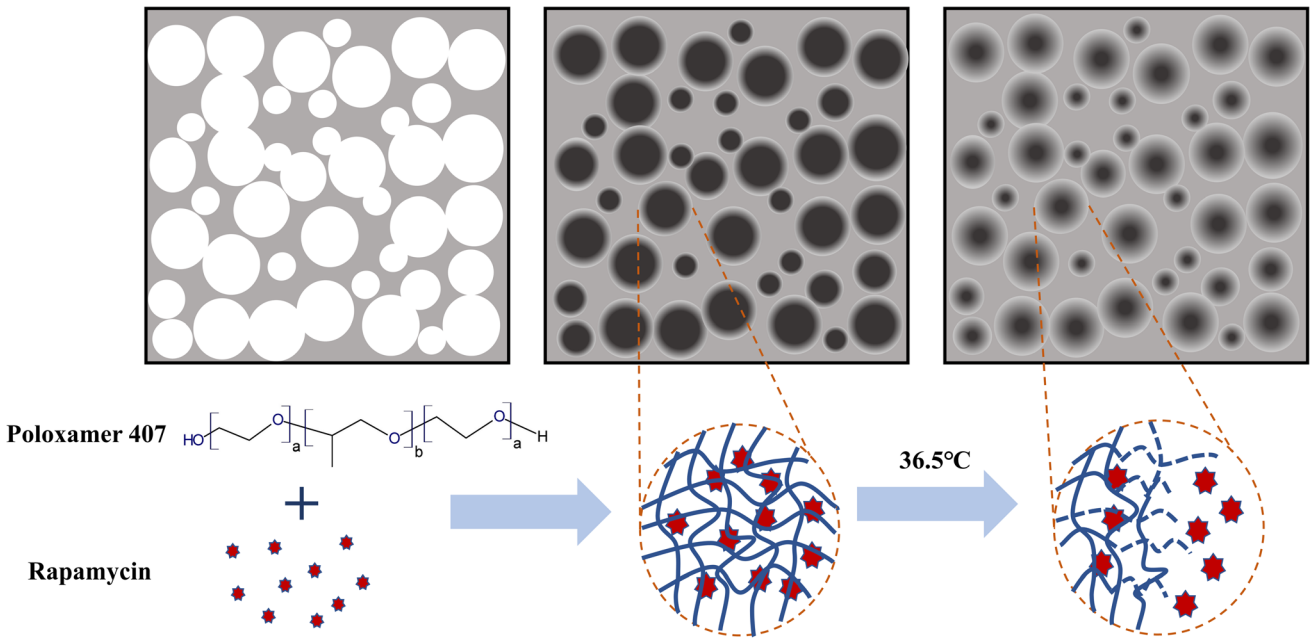

Fig. 10 Schematic illustrating the controlled release of rapamycin *via* erosion through the inner coating of the hydrogel. At low temperatures, the F127 hydrogel remains in a sol state, allowing efficient drug loading. Upon exposure to physiological temperatures (20–40 °C), the hydrogel transitions to a gel state owing to the self-assembly of PPO blocks, entrapping the drug within its network. The porous material further modulates the release kinetics by providing a sustained diffusion pathway for rapamycin, ensuring prolonged and controlled drug delivery.

NiTi. These findings indicate that higher porosity results in greater drug-loading capacity in porous NiTi. The drug release profiles of the porous NiTi implants were intrinsically linked to their pore architectures, as visualized by 3D-CT reconstructions (ESI Fig. 2–4†). Two distinct pore types were identified: Sintered Residual Pores (SRPs), submicron-sized (<1 μm) and isolated, contributed minimally to drug release due to their lack of connectivity; and space holder pores (SHPs), large interconnected networks formed by PMMA removal, which dominated drug loading and diffusion. N2 (20% porosity), characterized by moderate SHP interconnectivity, exhibited balanced release kinetics—35.9% initial elution at 1 day and 72.2% cumulative release over 13 days—reflecting efficient yet controlled diffusion through open channels. In contrast, N3 (40% porosity), despite its higher SHP volume[16] (389.7×10^6 μm^3 for P40-SHP), showed delayed initial release (30.3% at 1 day) and incomplete drug elution (68.2% at 31 days), likely due to tortuous pathways and partially isolated SHPs that impeded full drug accessibility. These findings highlight that, while increased porosity can significantly enhance drug-loading capacity and prolong the duration of sustained release, structural complexity, such as pore tortuosity or the presence of residual SRPs, may lead to a shielding effect, resulting in incomplete drug release. This mechanism warrants further investigation and validation. Building upon this foundation, while ensuring the high mechanical performance of porous NiTi alloy materials,[16] controlled internal pore structures can significantly enhance the drug-loading capabilities of Nitinol alloy.

To validate the functionality of the drug delivery platform within the vascular lumen, the proliferation of human smooth muscle cells (HUSMC) on these substrates was investigated. As the porosity of porous nickel-titanium (NiTi) materials increased, the cell number, accompanied by a diminished cell spreading area, exhibited a significant inhibitory trend. The anti-proliferative water-insoluble drug rapamycin was selected as a test drug to be loaded inside porous NiTi. Rapamycin plays a crucial role in maintaining vascular patency and preventing intimal hyperplasia and thrombosis through multiple mechanisms, thereby inhibiting the mTOR pathway and reducing smooth muscle and endothelial cell proliferation. Anti-inflammatory properties suppress leukocyte activation and cytokine release, whereas its antithrombotic effects reduce platelet aggregation. Additionally, rapamycin has antifibrotic properties that prevent scar tissue formation and help restore endothelial function, thereby ensuring vascular integrity and flexibility. These combined effects make rapamycin invaluable for drug-eluting stent applications. This includes but is not limited to antiproliferative drugs, anti-inflammatory agents, and antithrombotic agents.[32,33] In practice, any drug can be loaded into this system, including those with current or potential use in vascular lumen-related applications and bone therapy, such as anti-restenosis,[34] anticoagulant drugs,[35] antibacterial drugs[36], and so on.

This study investigated the therapeutic effects of porous NiTi implants loaded with Pluronic F127-rapamycin on neointimal hyperplasia in rat abdominal aortas. Implants with progressively increasing porosity exhibit corresponding enhancement in suppressing pathological vascular remodeling. In comparison with the N1 and N2 groups, the N3 group exhibited markedly reduced neointimal thickness and area. Additionally, the neointimal thickness in the N2 group was lower than that in

the N1 group. This therapeutic gradient was directly correlated with porosity-dependent drug loading capacity, where expanded porous architectures accommodated greater rapamycin payloads, thereby amplifying its inhibitory effect on smooth muscle cell proliferation. This result indicated that as the porosity increased, the amount of loaded rapamycin increased, resulting in a stronger inhibitory effect on neointimal hyperplasia. Higher porosity of Pluronic F127-rapamycin loaded porous NiTi resulted in a stronger inhibitory effect. This trend is consistent with the enhanced drug-loading capacity and sustained release kinetics of the porous architecture. Overall, these findings underscore the importance of tailoring NiTi's porous architecture to co-optimize mechanical integrity and drug-eluting performance, thereby providing a material-based framework for designing next-generation endovascular devices that integrate structural porosity with targeted pharmacological intervention.

The drug release characteristics of porous NiTi modified with thermosensitive hydrogels indicate that by adjusting the porosity, the drug release profile of porous NiTi implants can be tailored to the specific requirements of a given application, ensuring optimal therapeutic dosing within the desired timeframe. Thus, this approach offers flexibility and can be applied to NiTi implants for various purposes, ranging from short-term drug release scenarios, such as inflammation suppression, to mid-term (1–2 weeks) drug release scenarios, such as inhibiting early inflammatory responses, neointimal hyperplasia in vascular lumens, and in-stent restenosis.[37] Additionally, the interior of porous nickel-titanium can be utilized to load multiple drugs, providing a significantly higher drug loading capacity than traditional methods, thereby enabling the design of implants based on porous NiTi with multiple drug release capabilities for orthopedic and vascular applications. Tunable drug release profiles: pore interconnectivity promotes prolonged elution while maintaining therapeutic concentrations at the implantation site.

5. Limitation

Although the results of this investigation provide foundational insights into the applications of porous NiTi, several limitations warrant consideration. First, although animal models successfully demonstrated the material's drug-loading capacity and therapeutic efficacy, interspecies anatomical and physiological variations necessitate further validation in human trials to comprehensively evaluate its clinical potential and limitations in vascular surgery. Second, this study conducted an initial assessment of the porosity by evaluating dense NiTi in two porous configurations with porosities of 20.8% and 34.9%. To more thoroughly elucidate the relationship between porosity and material performance, future investigations should consider a wider range of porosity levels and various pore morphologies. Third, although rapamycin served as an effective model drug, the divergent physicochemical properties of other therapeutic agents may substantially influence the loading efficiency and release kinetics, demanding comparative pharmacotechnical characterization. Finally, although this study offers an initial exploration into the role of porosity, further investigations are warranted to examine a wider spectrum of porosity levels and to evaluate how varying pore structures influence the functional performance of nickel-titanium alloys.

6. Conclusion

In this study, we investigated the potential of porous NiTi alloys fabricated *via* Metal Injection Molding combined with the Powder Space-Holder method (MIM-PSH) as innovative drug delivery carriers. By integrating these materials with the thermosensitive PF127 hydrogel, we enhanced the loading and controlled release of the hydrophobic drug rapamycin. This combination leverages PF127's sol–gel transition properties under physiological conditions, optimizing the internal surface area of the porous NiTi matrix to achieve superior drug loading and sustained release profiles. Preliminary biocompatibility evaluations using human aortic smooth muscle cells (HASMC) and an aortic injury animal model indicate promising applications for this system in endovascular therapy.

Data availability

The authors confirm that all the data supporting the findings of this study are available within the article and its ESI file.†

Conflicts of interest

There are no conflicts to declare.

Acknowledgements

This work was supported by grants from the National Natural Science Foundation of China (Grant No. 81870345) and Postdoctoral Fellowship Program of CPSF (Grant No. GZC20233172).

References

1 B. Yuan, M. Zhu and C. Y. Chung, Biomedical porous shape memory alloys for hard-tissue replacement materials, *Materials*, 2018, **11**(9), 1716.
2 L. Petrini and F. Migliavacca, Biomedical applications of shape memory alloys, *J. Met.*, 2011, 2011.
3 L'H. Yahia, F. Rayes and A. O. Warrak, Regulation, orthopedic, dental, endovascular and other applications of Ti–Ni shape memory alloys, *Shape Memory Alloys for Biomedical Applications*, Woodhead Publishing, 2009, pp. 306–326.
4 R. Ma, Q. Liu, L. Zhou, *et al.*, High porosity 3D printed titanium mesh allows better bone regeneration, *BMC Oral Health*, 2023, **23**(1), 6, DOI: **10.1186/s12903-023-02717-5**.
5 Y. Zhou, T. Wang, P. Lu, *et al.*, Exploring the Potential of MIM-Manufactured Porous NiTi as a Vascular Drug Delivery Material, *Ann. Biomed. Eng.*, 2024, **52**(11), 2958–2974, DOI: **10.1007/s10439-024-03558-1**.

6 I. Rykowska, I. Nowak and R. Nowak, Drug-eluting stents and balloons—materials, structure designs, and coating techniques: a review, *Molecules*, 2020, **25**(20), 4624.
7 Z. He, Z. Wang, D. Wang, *et al.*, Microstructure and Mechanical Properties of Porous NiTi Alloy Prepared by Integration of Gel-Casting and Microwave Sintering, *Materials*, 2022, **15**(20), 7331.
8 M. Aftabi-Khadar, M. Adeli, M. Soltanieh, *et al.*, Pore Control in Porous NiTi Alloy Produced by Combustion Synthesis Method with the Utilization of Space Holders, *J. Mater. Eng. Perform.*, 2024, 1–12.
9 T. Bubpamala, P. Promoppatum and P. Pholpabu, Drug-releasing tannic acid-mediated adhesive PEG hydrogel for porous titanium implants, *ACS omega*, 2023, **9**(1), 887–895.
10 Z. Ma, Y. Zhao, Z. Xu, *et al.*, 3D-printed porous titanium rods equipped with vancomycin-loaded hydrogels and polycaprolactone membranes for intelligent antibacterial drug release, *Sci. Rep.*, 2024, **14**(1), 21749.
11 Y. T. Jian, Y. Yang, T. Tian, *et al.*, Effect of pore size and porosity on the biomechanical properties and cytocompatibility of porous NiTi alloys, *PLoS One*, 2015, **10**(6), e0128138.
12 S. Jacob, A. B. Nair, J. Shah, *et al.*, Emerging Role of Hydrogels in Drug Delivery Systems, Tissue Engineering and Wound Management, *Pharmaceutics*, 2021, **13**(3), 357, DOI: **10.3390/pharmaceutics13030357**.
13 S. Chatterjee, P. C. Hui and C. W. Kan, Thermoresponsive Hydrogels and Their Biomedical Applications: Special Insight into Their Applications in Textile Based Transdermal Therapy, *Polymers*, 2018, **10**(5), 480, DOI: **10.3390/polym10050480**.
14 C. Gong, T. Qi, X. Wei, *et al.*, Thermosensitive polymeric hydrogels as drug delivery systems, *Curr. Med. Chem.*, 2013, **20**(1), 79–94.
15 I. H. Abidi, F. A. Khalid, M. U. Farooq, *et al.*, Tailoring the pore morphology of porous nitinol with suitable mechanical properties for biomedical applications, *Mater. Lett.*, 2015, **154**, 17–20.
16 B. Zhu, D. Li, C. Du, *et al.*, Near-spherical micron-porous NiTi alloys with high performances fabricated *via* metal injection molding, *Mater. Sci. Eng. A*, 2024, **892**, 146114.
17 D. Li, J. Wang, C. Du, *et al.*, Technical explorations for manufacturing of NiTi unibody vascular stents through metal injection molding: materials performance, fatigue properties and biocompatibility, *Mater. Des.*, 2025, **250**, 113624.
18 S. C. Gupta, C. Sundaram, S. Reuter, *et al.*, Inhibiting NF-κB activation by small molecules as a therapeutic strategy, *Biochim. Biophys. Acta*, 2010, **1799**, 775–787.
19 K. Ohtani, K. Egashira, K. Nakano, G, *et al.*, Stent-based local delivery of nuclear factor-kappaB decoy attenuates in-stent restenosis in hypercholesterolemic rabbits, *Circulation*, 2006, **114**, 2773–2779.
20 E. M. Martín del Valle, M. A. Galan, *et al.*, Drug delivery technologies: the way forward in the new decade, *Ind. Eng. Chem. Res.*, 2009, **48**(5), 2475–2486.
21 S. Lee, C. H. Yoon and D. H. Oh, Gelatin microgel-coated balloon catheter with enhanced delivery of everolimus for long-term vascular patency, *Acta Biomater.*, 2024, **173**, 314–324.
22 P. J. R. Jaquilin, O. S. Oluwafemi, S. Thomas, *et al.*, Recent advances in drug delivery nanocarriers incorporated in temperature-sensitive Pluronic F-127–A critical review, *J. Drug Delivery Sci. Technol.*, 2022, **72**, 103390.
23 B. Shriky, A. Kelly, M. Isreb, M. Babenko, N. Mahmoudi, S. Rogers, O. Shebanova, T. Snow and T. Gough, Pluronic F127 thermosensitive injectable smart hydrogels for controlled drug delivery system development, *J. Colloid Interface Sci.*, 2020, **565**, 119–130.
24 F. Pluronic, Applications of thermo-reversible pluronic F-127 gels in pharmaceutical formulations, *J. Pharm. Sci.*, 2006, **9**(3), 339–358.
25 A. Pitto-Barry and N. P. E. Barry, Pluronic® block-copolymers in medicine: from chemical and biological versatility to rationalisation and clinical advances, *Polym. Chem.*, 2014, **5**(10), 3291–3297.
26 A. Varela-Moreira, Y. Shi, M. H. A. M. Fens, *et al.*, Clinical application of polymeric micelles for the treatment of cancer, *Mater. Chem. Front.*, 2017, **1**(8), 1485–1501.
27 S. Borhani, S. Hassanajili, T. S. H. Ahmadi, *et al.*, Cardiovascular stents: overview, evolution, and next generation, *Prog. Biomater.*, 2018, **7**, 175–205.
28 J. Kohn and J. Zeltinger, Degradable, drug-eluting stents: a new frontier for the treatment of coronary artery disease, *Expert Rev. Med. Devices*, 2005, **2**(6), 667–671.
29 J. Naghi, E. A. Yalvac, A. Pourdjabbar, *et al.*, New developments in the clinical use of drug-coated balloon catheters in peripheral arterial disease, *Med. Devices: Evidence Res.*, 2016, 161–174.
30 R. A. Byrne, M. Joner, F. Alfonso, *et al.*, Drug-coated balloon therapy in coronary and peripheral artery disease, *Nat. Rev. Cardiol.*, 2014, **11**(1), 13–23.
31 I. Schorn, H. Malinoff, S. Anderson, *et al.*, The Lutonix® drug-coated balloon: A novel drug delivery technology for the treatment of vascular disease, *Adv. Drug Deliv. Rev.*, 2017, **112**, 78–87.
32 S. O. Marx, T. Jayaraman, L. O. Go, *et al.*, Rapamycin-FKBP inhibits cell cycle regulators of proliferation in vascular smooth muscle cells, *Circ. Res.*, 1995, **76**(3), 412–417.
33 M. C. Morice, P. W. Serruys, J. E. Sousa, *et al*, Randomized Study with the Sirolimus-Coated Bx Velocity Balloon-Expandable Stent in the Treatment of Patients with *de Novo* Native Coronary Artery Lesions. A randomized comparison of a sirolimus-eluting stent with a standard stent for coronary revascularization, *N. Engl. J. Med.*, 2002, **346**(23), 1773–1780.
34 E. Regar, G. Sianos and P. W. Serruys, Stent development and local drug delivery, *Br. Med. Bull.*, 2001, **59**(1), 227–248.
35 J. Kohn and J. Zeltinger, Degradable, drug-eluting stents: a new frontier for the treatment of coronary artery disease, *Expert Rev. Med. Devices*, 2005, **2**(6), 667–671.
36 P. A. Tran, L. Sarin, R. H. Hurt, *et al.*, Opportunities for nanotechnology-enabled bioactive bone implants, *J. Mater. Chem.*, 2009, **19**(18), 2653–2659.
37 F. G. P. Welt and C. Rogers, Inflammation and restenosis in the stent era, *Arterioscler., Thromb., Vasc. Biol.*, 2002, **22**(11), 1769–1776.